Supporting information

Enhanced interface reactivity by nanowrinkled functional layer for intermediate-temperature solid oxide fuel cells

Jongseo Lee[†], Sangyeon Hwang[†], Minwoo Ahn[†], Mingi Choi, Seungwoo Han, Doyoung Byun[*], and Wonyoung Lee[*]

Department of Mechanical Engineering, Sungkyunkwan University, Suwon 16419, Republic of Korea

[*] Corresponding authors. E-mails: dybyun@skku.edu and leewy@skku.edu

[†] These authors contributed equally to this study

List of Contents:

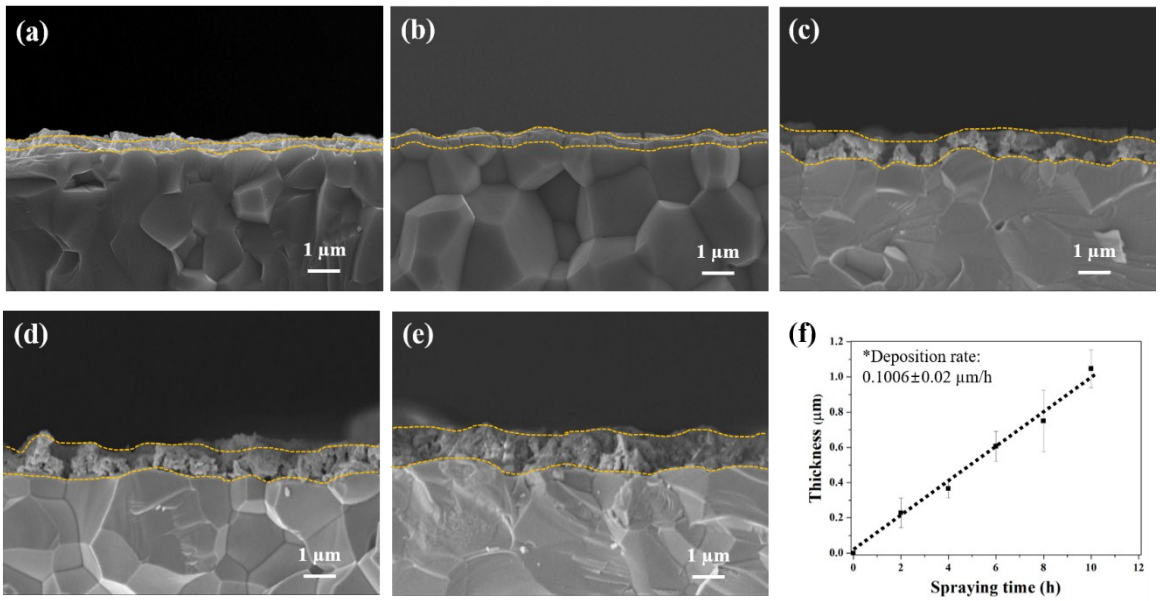

Figure S1. SEM images of the nanowrinkled functional layers with the thicknesses of (a) 0.2, (b) 0.4, (c) 0.6, (d) 0.8, and (e) 1 μm. (f) Deposition rate of the nanowrinkled functional layer.

Figures S1(a–e) show cross-sectional SEM images of the nanowrinkled functional layers with different thicknesses on the GDC substrate. Figure S1(f) shows the nanowrinkled functional layer thickness as a function of the deposition time. The nanowrinkled functional layer thickness exhibited a linear relation with the deposition time; the deposition rate was -0.1 μm/h.

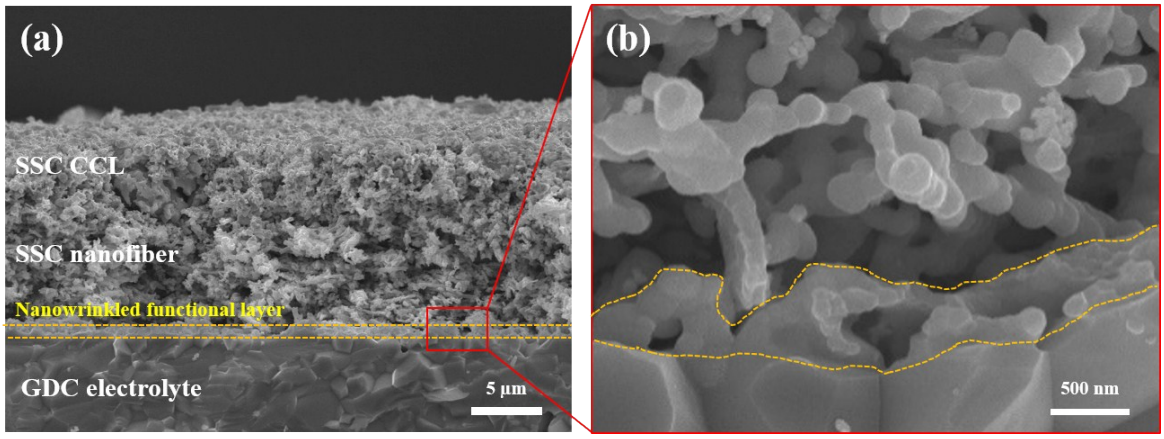

Figure S2. Cross-sectional SEM images for (a) the 0.6 FL electrode and (b) adopted nanowrinkled functional layer.

Figure S2(a) shows a cross-sectional SEM image of the 0.6 FL electrode consisting of the SSC current collecting layer (SSC CCL), SSC nanofiber, and nanowrinkled functional layer on the GDC electrolyte. In Figure S2(b), the nano-wrinkled functional layer can be observed at the interface between the nanofiber electrode and the electrolyte. The SSC nanofiber and the nano-wrinkled functional layer showed good contacts with each other.

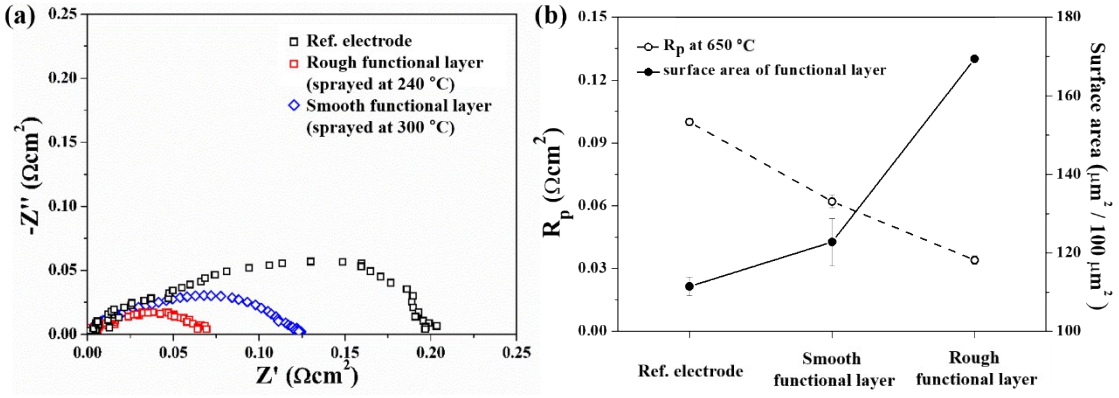

Figure S3. (a) Impedance spectra of the Ref. and FL electrodes with smooth and rough functional layers. (b) Polarization resistance and surface area of the nanowrinkled functional layer of each cell.

To demonstrate the effect of the surface morphology of the nanowrinkled functional layer on the polarization resistance, two distinct structures were employed at the interface between the nanofiber electrode and electrolyte. As described in the main article, the structure of the functional layer could be designed by the heating temperature. At a high temperature (300 °C), a smooth structure could be fabricated, as shown in Figure 1. On the contrary, a rougher structure was fabricated at a low temperature (240 °C). The Nyquist plot in Figure S3 shows the electrode resistance difference with respect to the interfacial surface area, while the grain size effect is common for both smooth and rough functional layers. The surface areas measured by AFM are 169.41 ± 0.8 and 122.76 ± 6 μm^2 for the structures heated at 240 and 300 °C, respectively. According to the comparison of the rough and smooth functional layers, the decreased polarization resistance from 0.1 to 0.0625 Ωcm^2 indicates the enhanced ORR at grain boundaries in the functional layer. Considering the surface roughness difference between the smooth and rough interfacial layers, the polarization resistance decreased from 0.0625 to 0.034 Ωcm^2, showing the improved electrode reaction with an increased number of reaction sites.

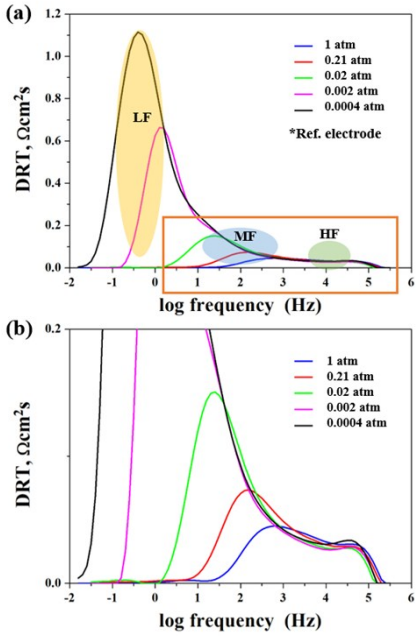

Figure S4. DRT plot of Ref. electrode as a function of the frequency at different pO_2 values in the range of 0.0004–1 atm.

To identify the peaks in the Bode plot precisely, a systematic DRT analysis was carried out. Figure S4(a) shows overall plots, while Figure S4(b) shows a magnified view of the red box in Figure S4(a). Three distinct peaks were identified in the LF, MF, and HF ranges. The peaks in the HF range are unaffected by the change in pO_2, while the peaks in the HF and MF ranges are dependent on pO_2. The DRT analysis showing the three different peaks is presented in detail in the manuscript.

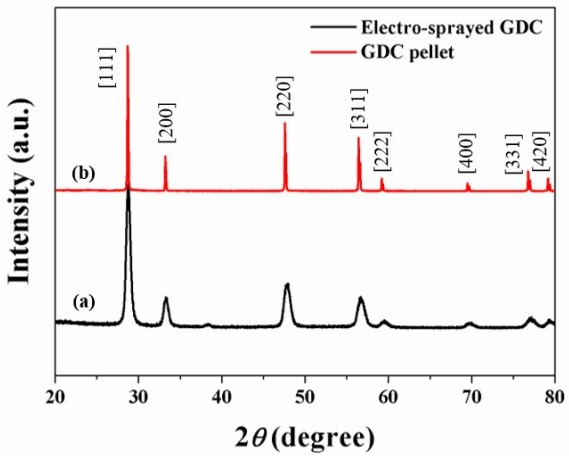

Figure S5. XRD patterns of the (a) nanowrinkled functional layer with a thickness of 0.8 μm and (b) electrolyte pellet.

Figure S5 shows the diffraction patterns of the nanowrinkled functional layer and electrolyte pellet sintered at 900 °C for 3 h and at 1500 °C for 5 h, respectively. Both samples exhibited the cubic fluorite phase without detectable impurities. The average grain sizes of both samples were calculated using the XRD patterns by the Scherrer's equation[1]:

$$D = \frac{0.9\,\lambda}{B\cos\theta} \qquad (1)$$

where D is the grain size, λ is the wavelength of the X-ray (0.154 nm), B is the full width at half maximum, and θ is the diffraction angle. The calculated grain size of the nanowrinkled functional layer (25 ± 5 nm) was approximately two orders of magnitude smaller than that of the electrolyte pellet (2 ± 0.5 μm), which confirms that the nanowrinkled functional layer had a higher (approximately two orders of magnitude) density of grain boundaries than that of the electrolyte pellet.

Table S1. Contributions of the resistances associated with the three frequencies to the total resistance measured at 650 °C.

	$R_{LF, MF, HF}$ contributions to the total R_p (%)						
	Ref.	0.2 FL	0.4 FL	0.6 FL	0.8 FL	1 FL	Average
LF	0.00574 (5.83%)	0.00604 (7.14%)	0.00731 (11.03%)	0.00612 (17.62%)	0.00521 (16.05%)	0.00534 (15.76%)	12.24
MF	0.0576 (58.60%)	0.0537 (63.47%)	0.0406 (61.21%)	0.0190 (54.77%)	0.0175 (53.99%)	0.0188 (55.33%)	57.90
HF	0.035 (35.56%)	0.0249 (29.39%)	0.0184 (27.77%)	0.00957 (27.58%)	0.00188 (29.95%)	0.00980 (28.86%)	29.85

Table S1 shows the contributions of the R_p values associated with the three frequency ranges defined by the DRT analysis to the total R_p. The contribution of R_{LF} seems to increase with the nanowrinkled functional layer thickness, although the absolute R_{LF} remains almost unchanged, as the absolute R_{MF} and R_{HF} are significantly decreased, as shown in Table S1 and Figure 4(c). For all samples, R_{MF} dominantly contributes to the total R_p with an average value of 57.9%. R_{HF} contributes to the total R_p with an average value of 29.58%. These results show that both R_{MF} and R_{HF} dominantly contribute to the total R_p with an average value of 87.75% even though the absolute R_{MF} and R_{HF} are significantly decreased.

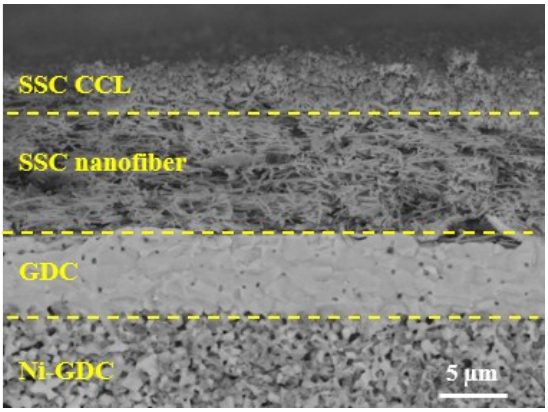

Figure S6. Cross-sectional SEM image of the Ni–GDC anode-supported full cell.

Figure S6 shows a cross-sectional SEM image of the Ni–GDC anode-supported full cell. The thicknesses of the Ni–GDC anode and GDC electrolyte were -700 and 7 μm, respectively. The porous anode allowed sufficient supply of reactant H_2 gas, while the GDC electrolyte formed the dense film to separate the gases between the two electrode sides. The cathode layer was fabricated by the same process described in the article.

Reference

1. M. Zhi, S. Lee, N. Miller, N. H. Menzler and N. Wu, *Energy Environ. Sci.*, 2012, **5**, 7066-7071.